Supplementary Materials for

Wireless, battery-free, subdermally implantable platforms for transcranial and long-range optogenetics in freely moving animals

Jokubas Ausra, Mingzheng Wu, Xin Zhang, Abraham Vázquez-Guardado, Patrick Skelton, Roberto Peralta, Raudel Avila, Thomas Murickan, Chad R. Haney, Yonggang Huang, John A. Rogers*, Yevgenia Kozorovitskiy*, Philipp Gutruf*

*Corresponding author. Email: pgutruf@email.arizona.edu, yevgenia.kozorovitskiy@northwestern.edu, jrogers@northwestern.edu

The PDF file includes:

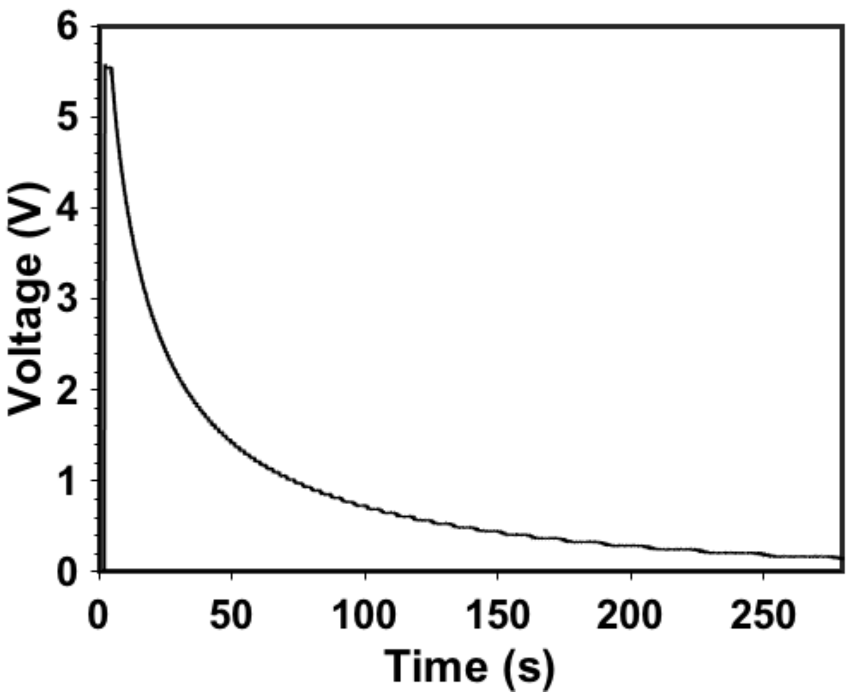

Fig. S1. Discharge of 176 μF capacitor bank over 1 MΩ resistor.

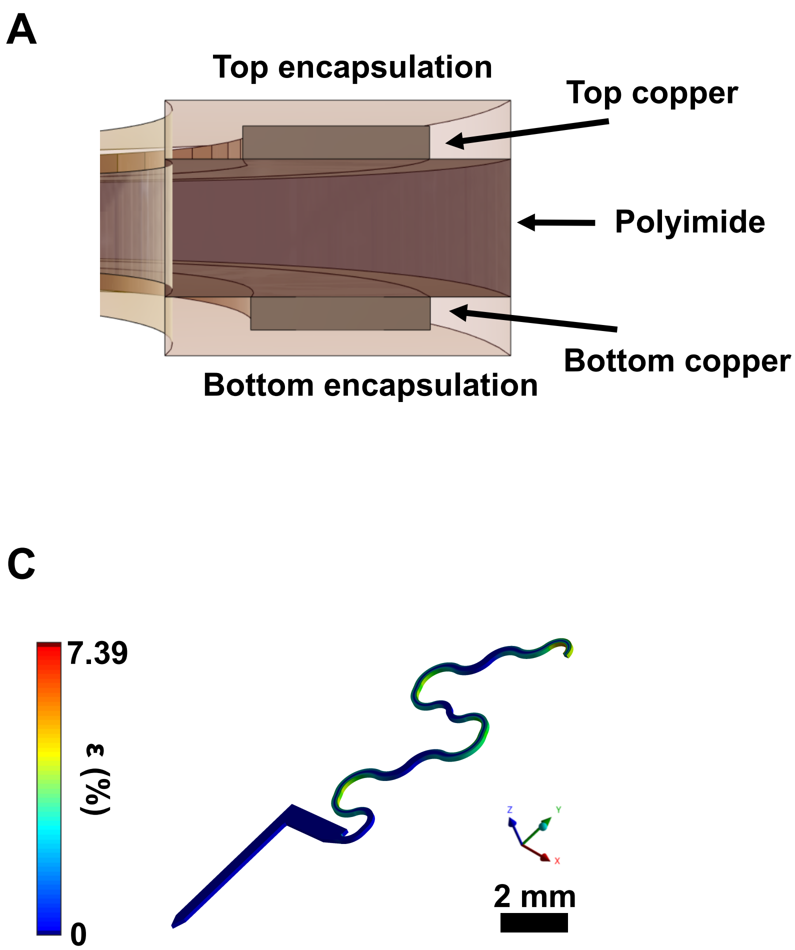

Fig. S2. Mechanical characterization of long-range device. The serpentine experiences a maximum displacement of 5.53 mm (110%). **(A)** Cross-sectional schematic of serpentine layers. **(B)** Direction of displacement indicated with arrow (point B) and location of fixed support (point A). **(C)** Isometric view of serpentine with polyimide exposed. **(D)** Isometric view of serpentine with copper exposed.

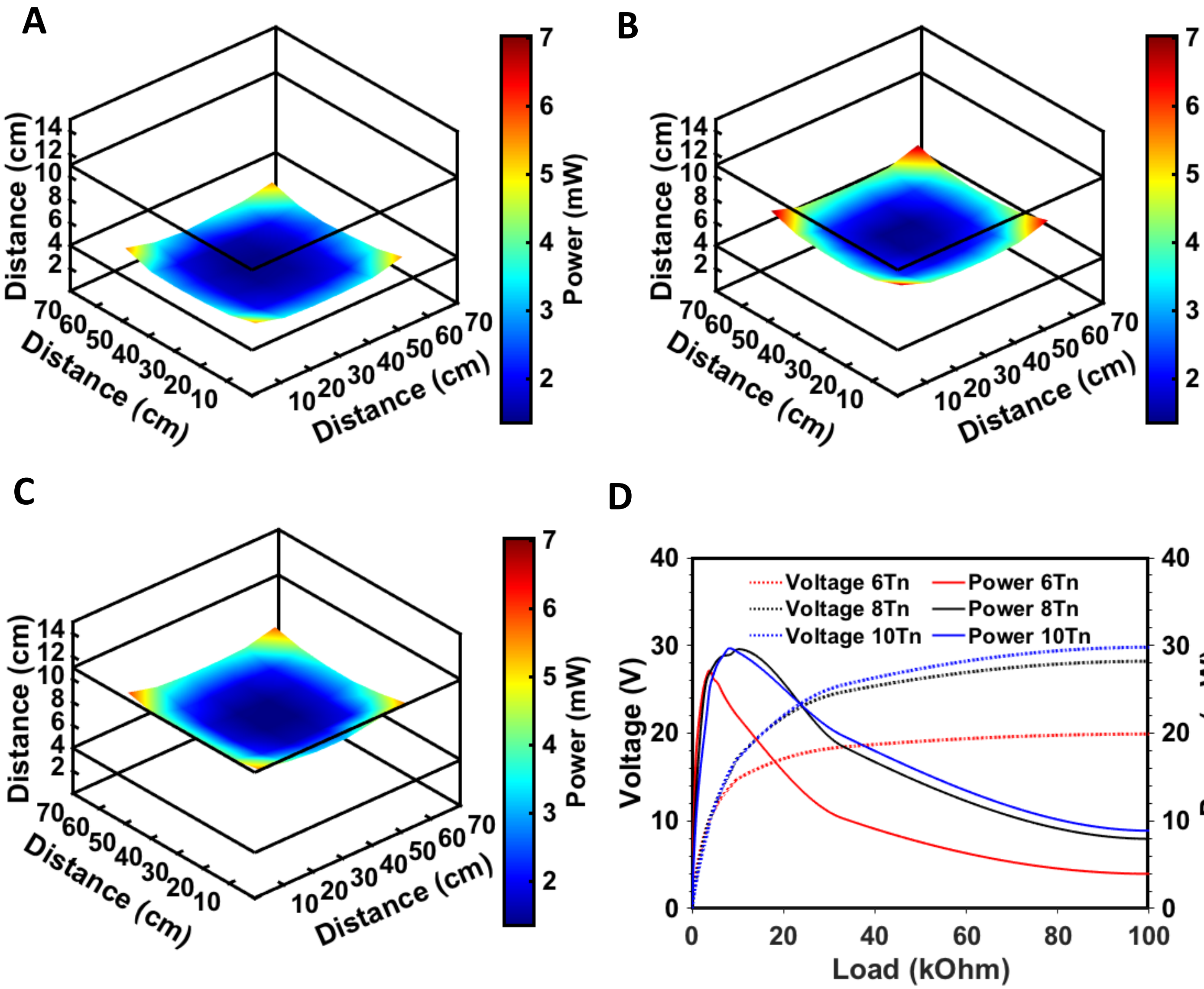

Fig. S3. Power characterization of a long-range device. Experimentally measured power maps in a 70 x 70 cm cage are shown at heights of **(A)** 3 cm, **(B)** 6 cm, and **(C)** 8 cm. **(D)** Rectification behavior of a long-range device with 6, 8 and 10 turns in the center of a 30 cm x 30 cm arena at a height of 3 cm from the arena floor with an input power of 8 W.

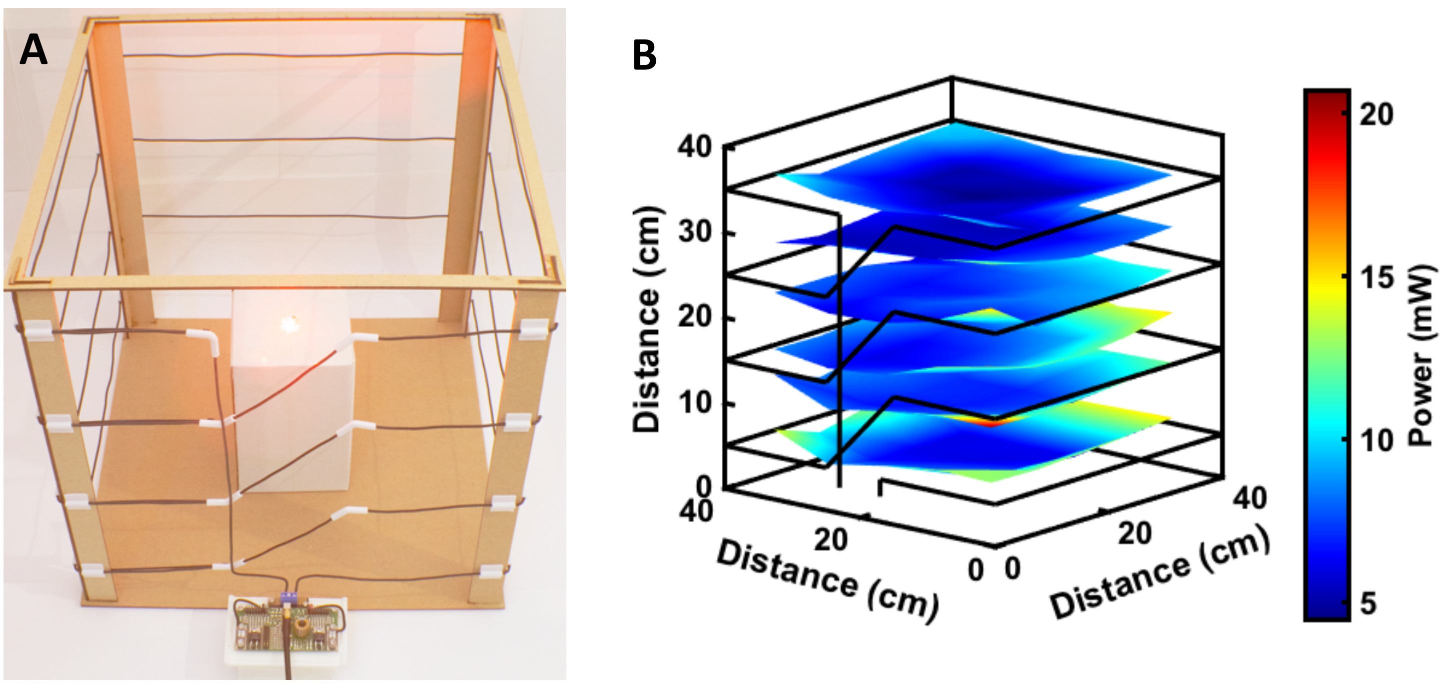

Fig. S4. Long distance device operation in a 40 x 40 x 40 cm arena. (A) Photograph of the device in operation. **(B)** Power harvesting characterization of device with RF input power of 8 W.

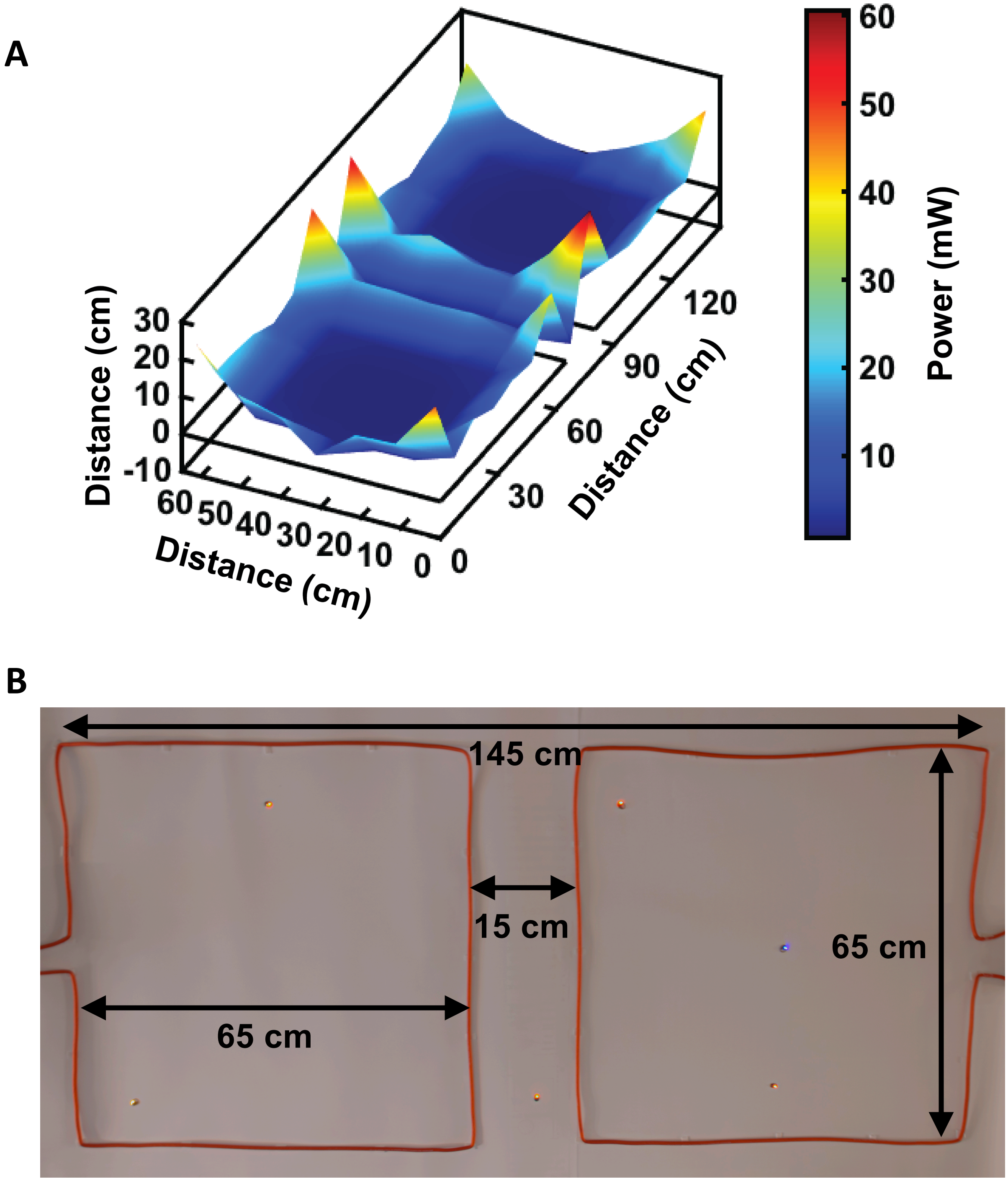

Fig. S5. Demonstration of long-range device operation over larger areas. (A) Power distribution map of a long-range device on the floor of two 65 x 65 cm cages separated by 15 cm with an input power of 10 W respectively. **(B)** Photographic image of six devices activated an arena comprised of two 65 x 65 cm cages.

Fig. S6. Photographic image of a transcranial device activated on 3D printed skull.

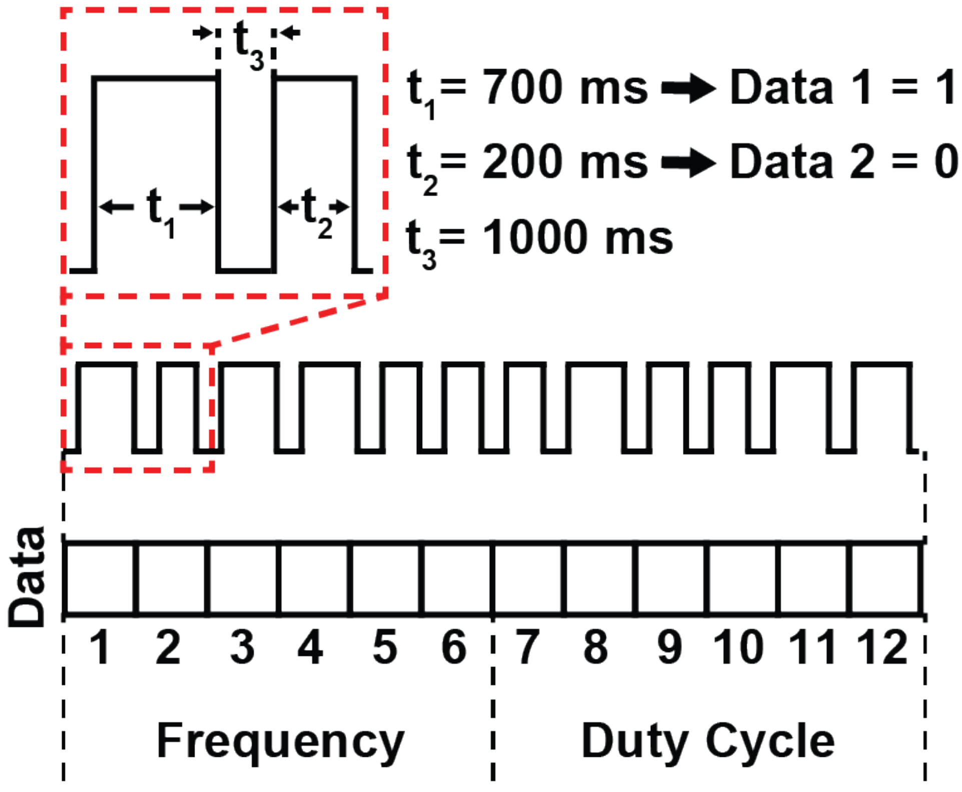

Fig. S7. Protocol for state selection using 12 bits of data to select device frequency and duty cycle.

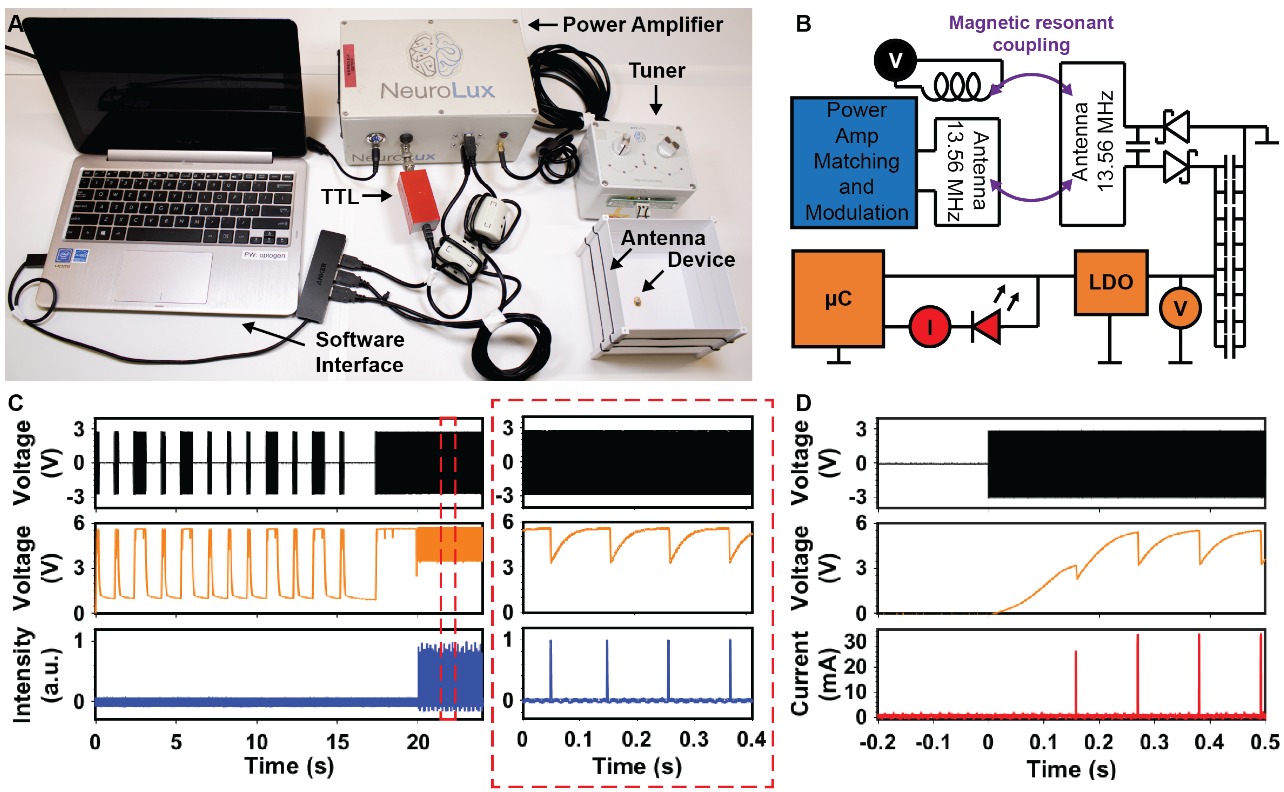

Fig. S8. Programming and low latency startup of high intensity stimulation device. (A) Photographic image of equipment used to generate pulses for device programming. **(B)** Simplified electronic diagram for the high intensity device. **(C)** Graph of pickup coil indicating RF pulses (black trace), voltage across capacitor bank (orange trace) and intensity of μ-ILED (blue trace) with inset showing traces over four stimulation cycles. **(D)** Graph of pickup coil voltage indicating RF field startup (black trace), voltage across capacitor bank (orange trace), and current through μ-ILED (red trace) for the high intensity device.

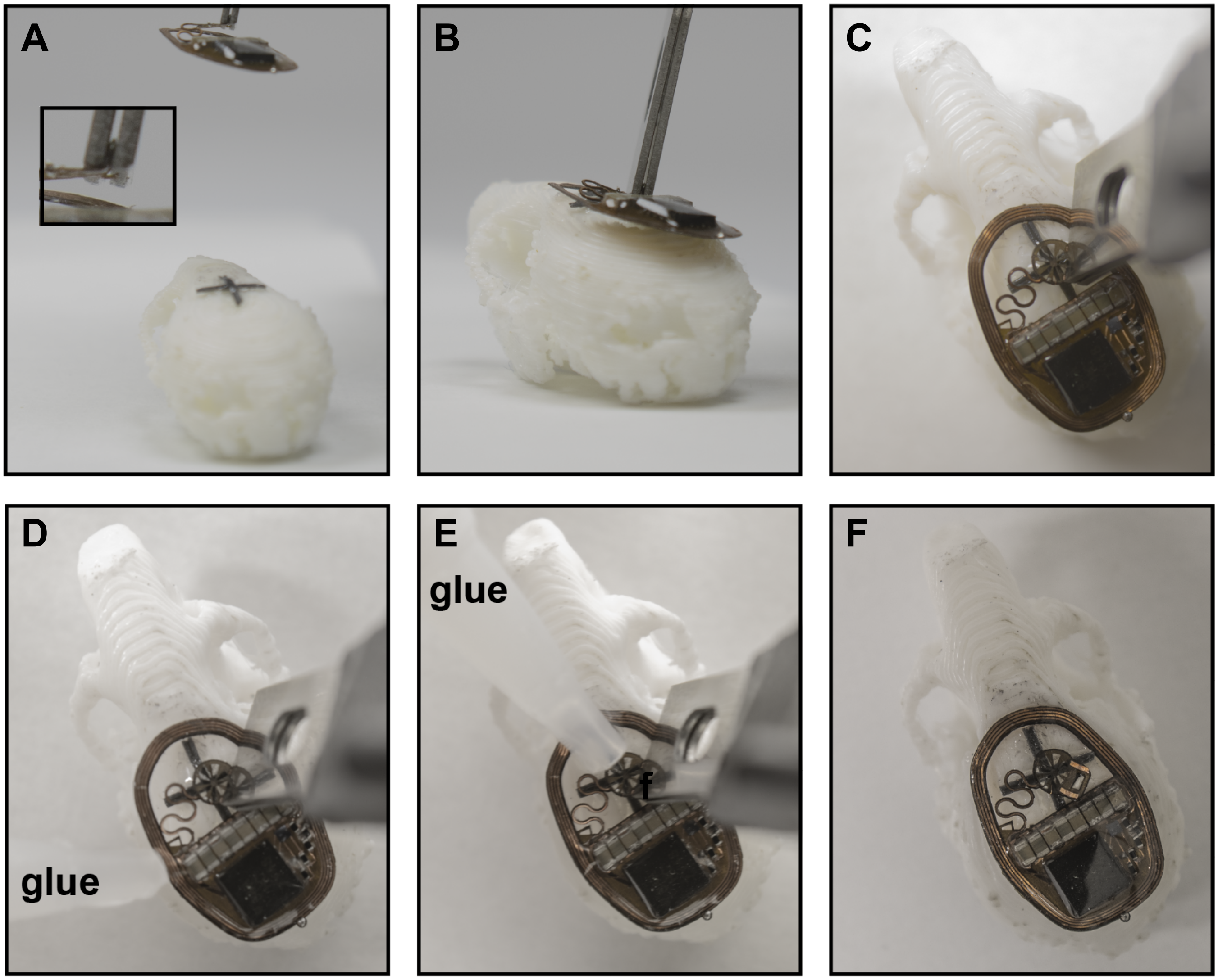

Fig. S9. Implantation procedure of a transcranial device. (A) Side view photographic image of device placed over skull with stereotactic setup and inset showing tab bent to 90 degrees. **(B)** Side view photographic image of device being lowered onto target with stereotactic setup. **(C)** Top view photographic image of device being positioned on target. **(D)** Top view photographic image of device antenna being glued onto skull. **(E)** Top view photographic image of stimulation pad put into place and glued. **(F)** Top view photographic image of stimulation pad tab bent to 0 degrees.

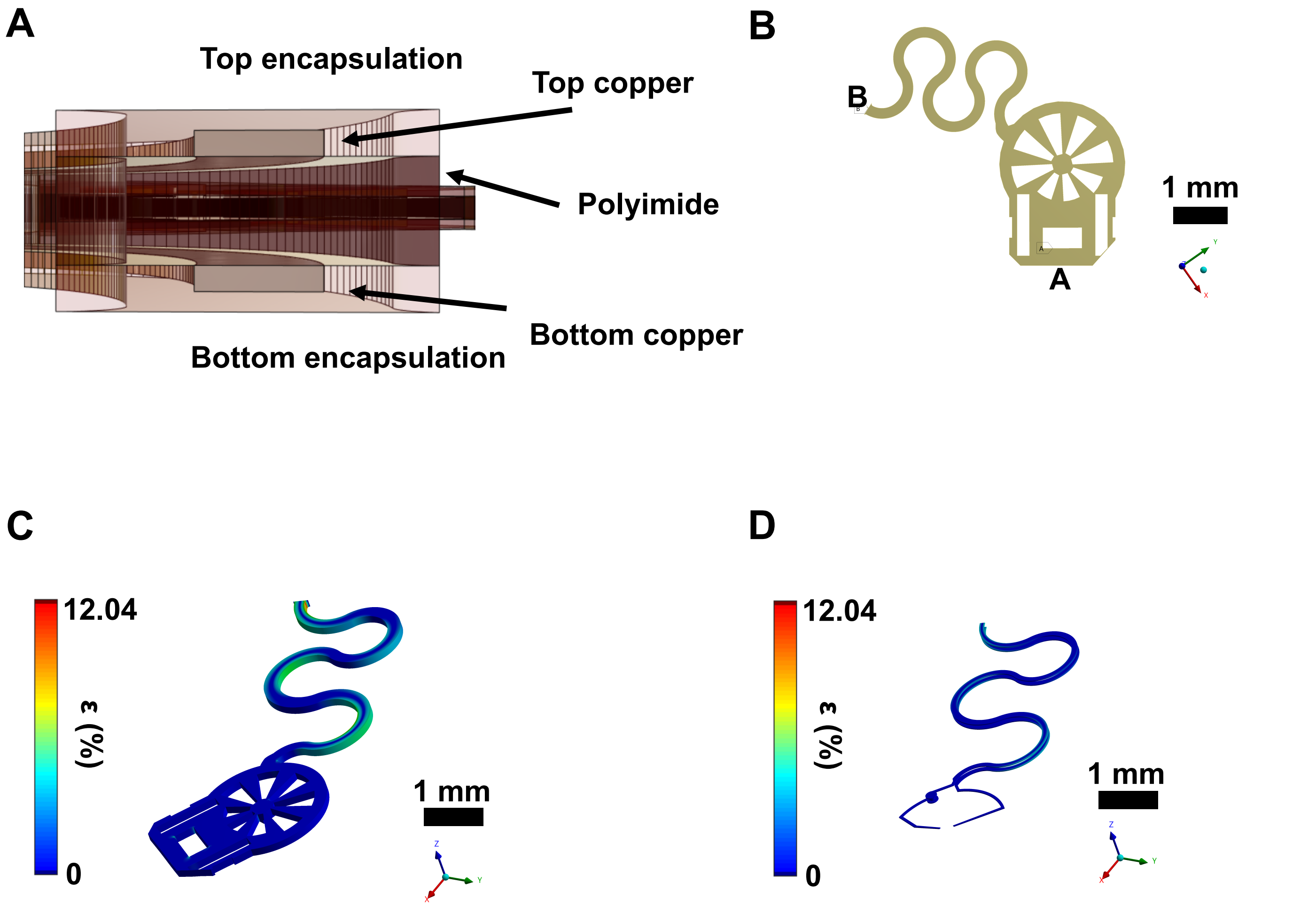

Fig. S10. Mechanical characterization of transcranial device. The serpentine experiences a maximum displacement of 2.05 mm (75%). **(A)** Cross-sectional schematic of serpentine layers. **(B)** Direction of displacement indicated with arrow (point B) and location of fixed support (point A). **(C)** Isometric view of serpentine with polyimide exposed. **(D)** Isometric view of serpentine with copper exposed.

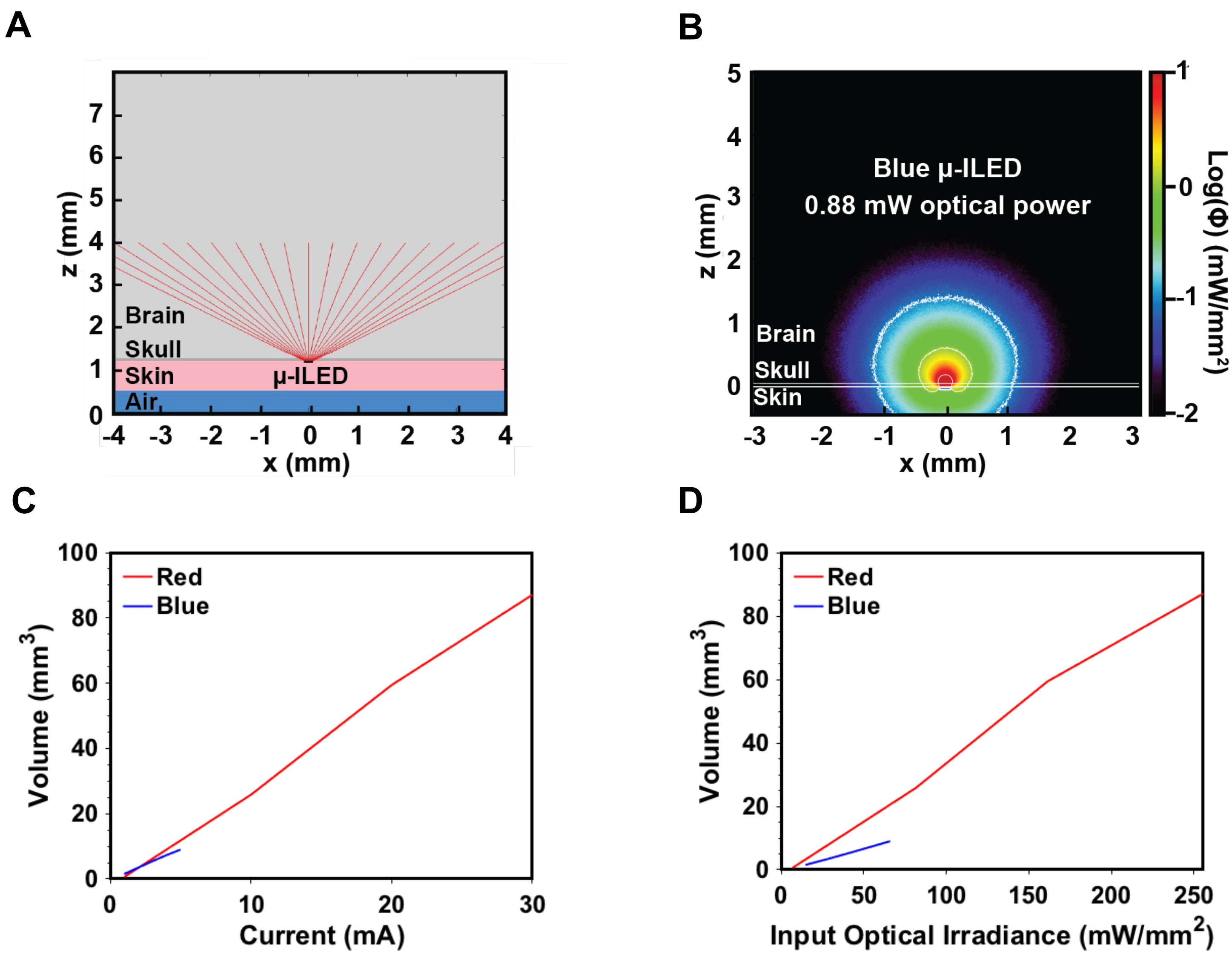

Fig. S11. Monte Carlo optical simulations scheme and results. (A) Materials used in Monte Carlo simulations. **(B)** Light penetration measured by irradiance through skull and brain with blue μ-ILED with 0.88 mW optical power. **(C)** Illumination volume with increasing input current for red and blue μ-ILED. **(D)** Illumination volume with increasing optical irradiance for red and blue μ-ILED.

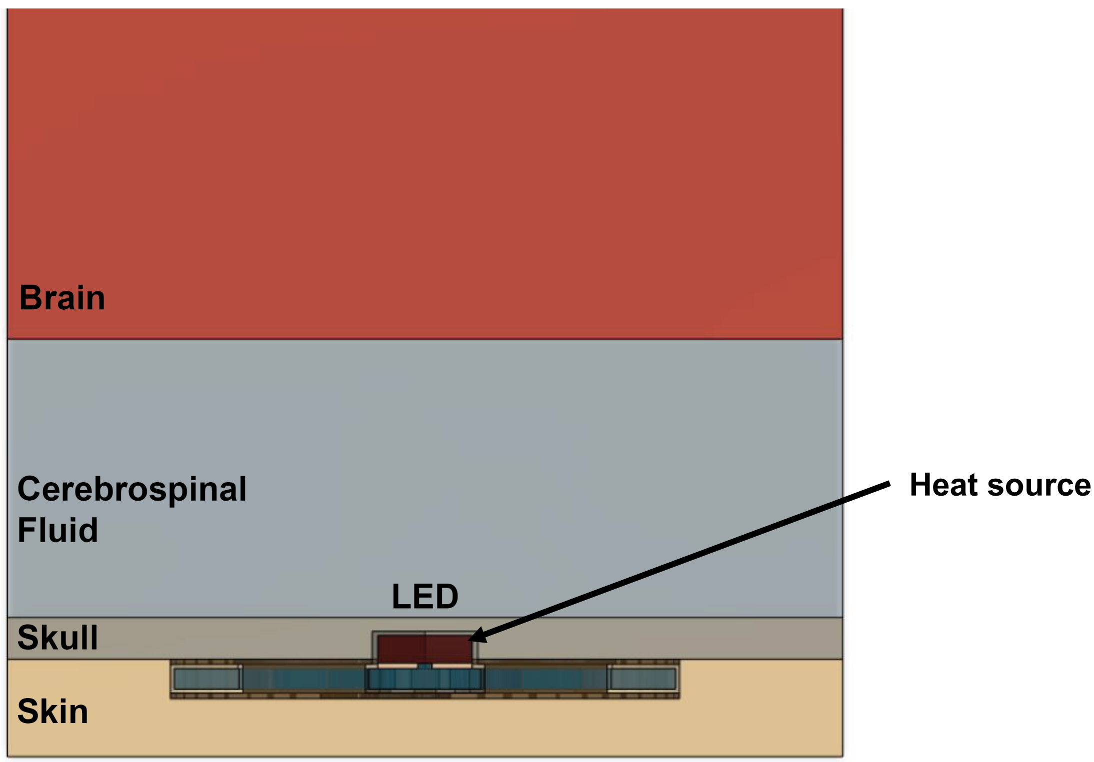

Fig. S12. Finite element analysis setup for steady state and transient thermal simulations.

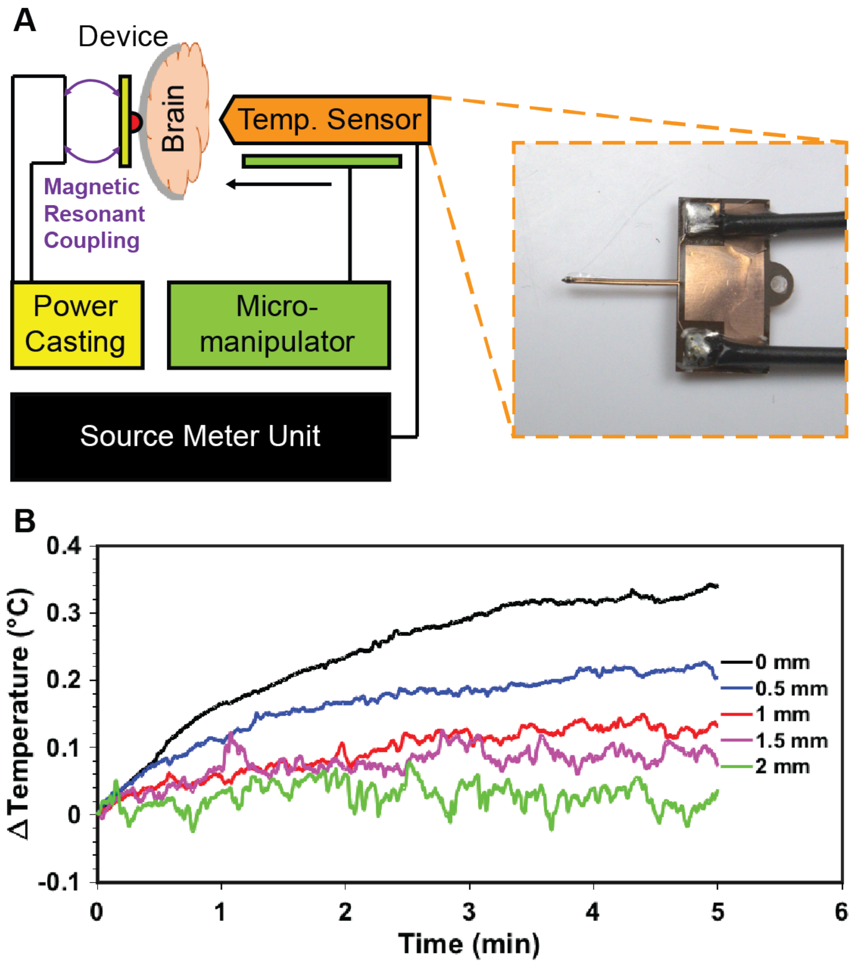

Fig. S13. Experimentally measured transcranial thermal propagation. (A) Schematic setup used for brain temperature measurements with the inset showing the temperature probe. **(B)** Sample increase in temperature of μ-ILED using the custom built temperature measurement apparatus. Legend indicates brain depth from the μ-ILED.

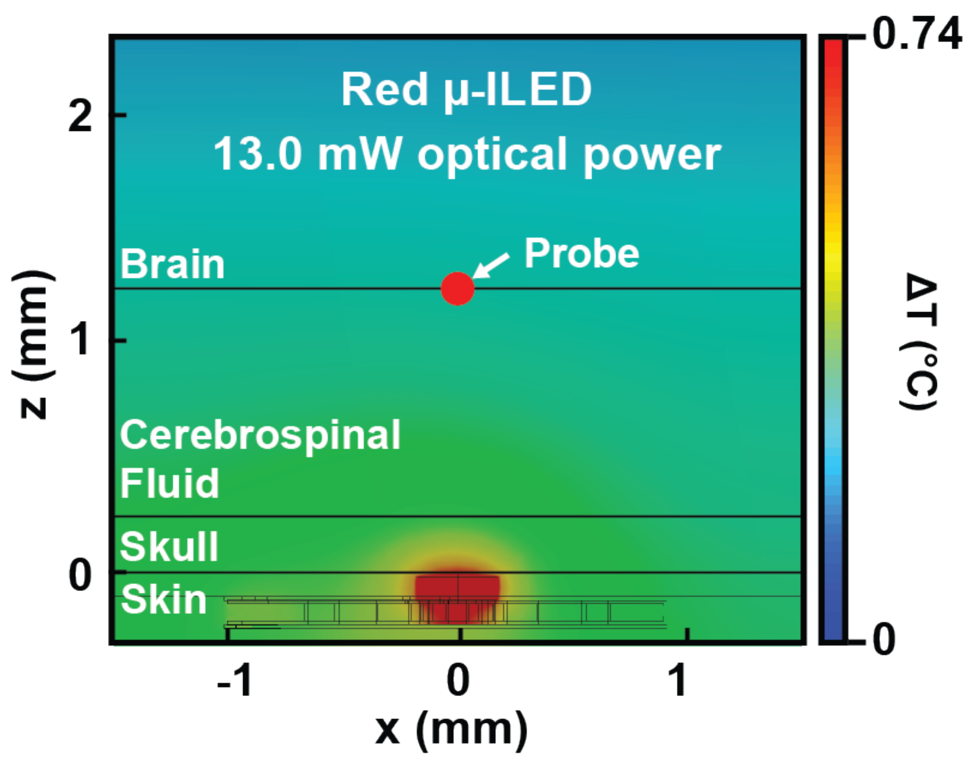

Fig. S14. Steady state thermal impact analysis of red μ-ILED operated at 13 mW for skull thickness of 250 μm. A temperature of 0.25 °C is observed at the probe located at the brain/CSF interface.

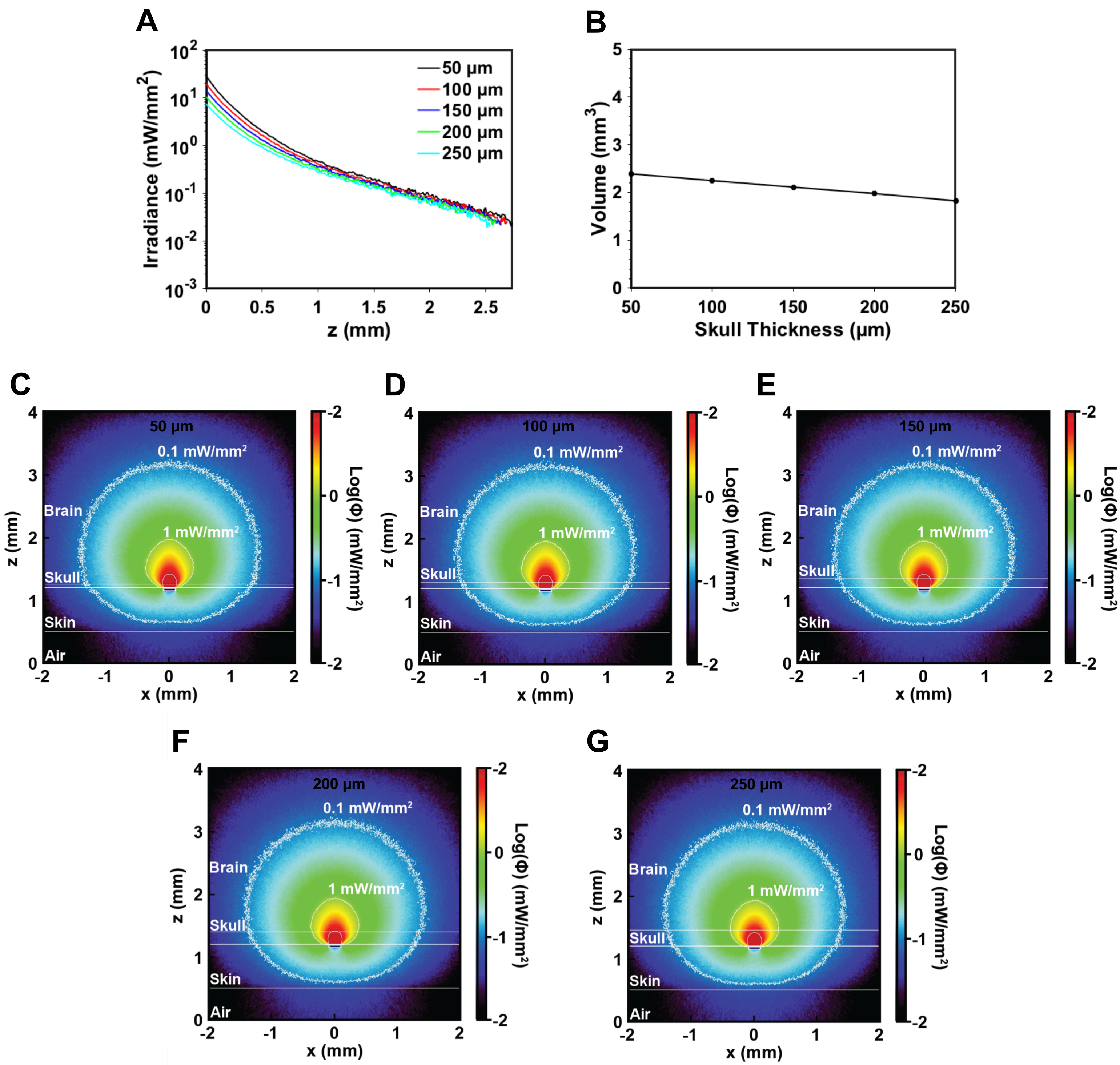

Fig. S15. Monte Carlo optical simulation results for red µ-ILED with varying skull thickness. (A) Irradiance measurements for mouse skull and brain for red µ-ILED at 1 mW optical power with varying skull thickness. **(B)** Brain illumination volume for red µ-ILED at 1 mW optical power with varying skull thickness. **(C)** Monte Carlo simulations of light propagation through skull for a red light source with 1 mW optical power and skull thickness of 50 µm, **(D)** 100 µm, **(E)** 150 µm, **(F)** 200 µm, **(G)** 250 µm.

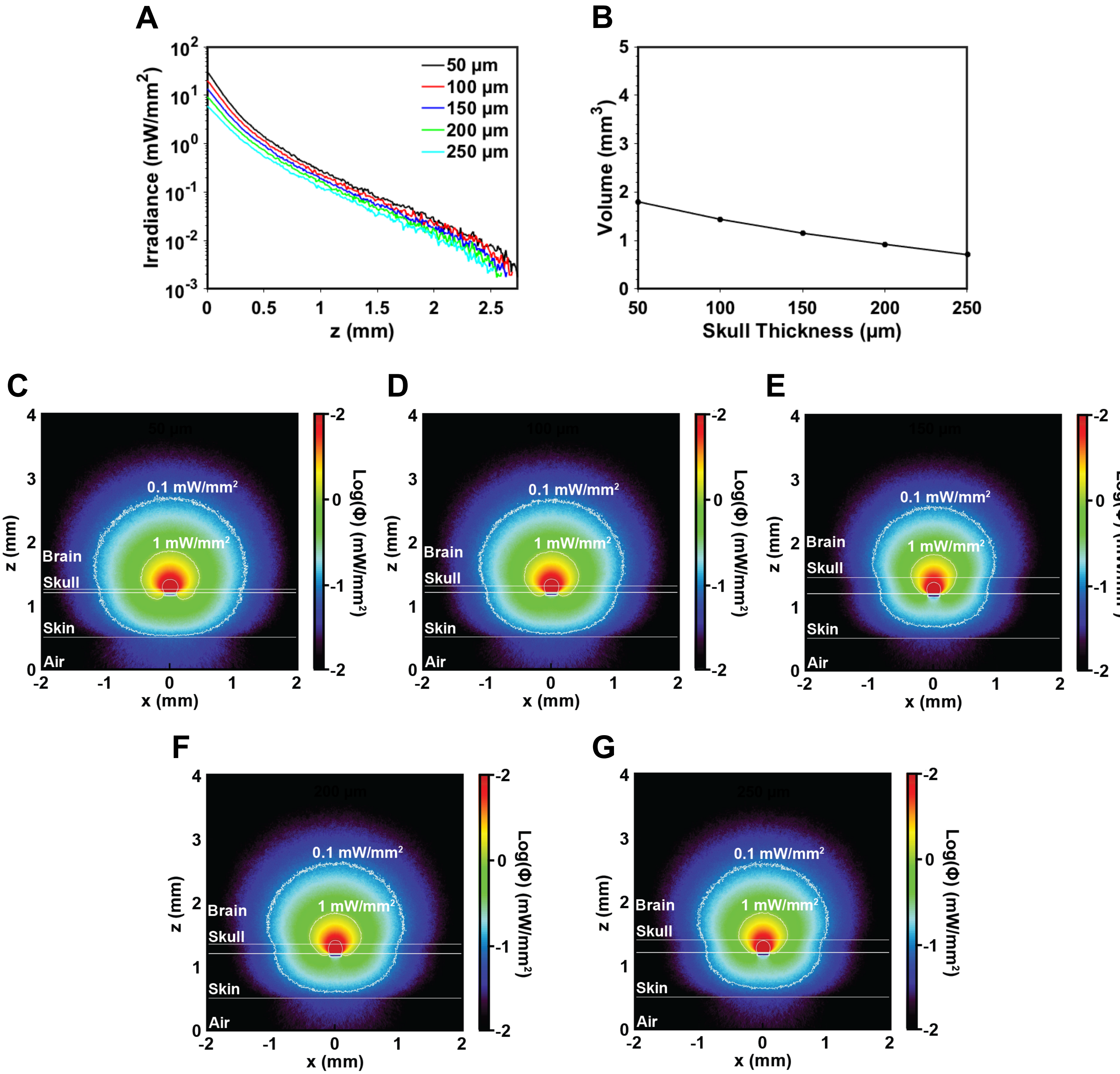

Fig. S16. Monte Carlo optical simulation results for blue µ-ILED with varying skull thickness. **(A)** Irradiance measurements for mouse skull and brain for blue µ-ILED at 1 mW optical power with varying skull thickness. **(B)** Brain illumination volume for blue µ-ILED at 1 mW optical power with varying skull thickness. **(C)** Monte Carlo simulations of light propagation through skull for a blue light source with 1 mW optical power and skull thickness of 50 µm, **(D)** 100 µm, **(E)** 150 µm, **(F)** 200 µm, **(G)** 250 µm.

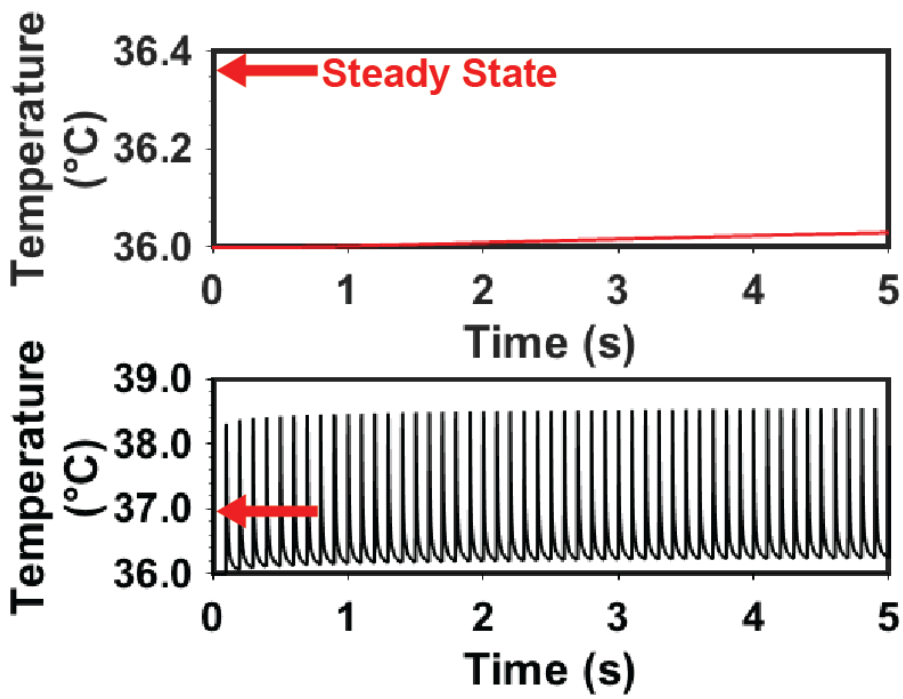

Fig. S17. Transient and steady state Finite element stimulation. Transient thermal impact simulation of red μ-ILED stimulation at 13 mW optical power and 10 Hz at CSF/brain interface (top) and μ-ILED/skull interface (bottom) with arrows indicating steady state temperature.

Antenna Dimensions (L x W x H)	Self-resonance-frequency (MHz)	Real (Z) at 13.56 MHz	Imaginary (Z) at 13.56 MHz
300 x 300 x 150 mm	48.10	1.45	230.7
400 x 400 x 150 mm	31.73	2.92	340.8
500 x 500 x 150 mm	24.90	8.22	528.9
600 x 600 x 150 mm	21.20	21.7	823
700 x 700 x 150 mm	19.10	50.2	1237
800 x 800 x 150 mm	15.94	263	2583
900 x 900 x 150 mm	14.25	2826	7864
1000 x 1000 x 150 mm	12.63	1595	-5754

Table S1. Table showing self resonance computed for increasing arena sizes.

Color	μ_a (cm^{-1})^{REF}				μ_s (cm^{-1})^{REF}				g^{REF}			
	Brain (WM)	Brain (GM)	Skull	Skin	Brain (WM)	Brain (GM)	Skull	Skin	Brain (WM)	Brain (GM)	Skull	Skin
BLUE	1.2[37]	0.6[37]	12[38]	1.8[39]	420[37]	120[37]	236[40]	139[40]	0.8[40]	0.88[37]	0.9[40]	0.65[40]
RED	0.8[37]	0.2[37]	0.4[38]	0.8[39]	400[37]	90[37]	189[40]	211[40]	0.84[40]	0.9[37]	0.9[40]	0.85[40]

Table S2. Optical parameters used for the numerical simulations. Absorption coefficient μa, scattering coefficient μs, and dissymmetry factor g. Brain white matter (WM). Brain grey matter (GM).

Movie S1. Freely moving mouse during active stimulation with long-range device in 50 x 50 cm arena.

Movie S2. Demonstration of high intensity device wireless programmability.

Movie S3. Thermal simulation of red μ-ILED on thinned skull operated at 10 Hz and 13 mW optical power.

Movie S4. Unilateral wireless transcranial optogenetic stimulation in mouse subject with thinned skull tracked with Deeplabcut.

Movie S5. Unilateral wireless transcranial optogenetic stimulation in M2 produces robust rotational behaviors in mice expressing ChrimsonR with fully intact skulls.